# Chapter 15
# The Use of Numerical Flow and Transport Models in Environmental Analyses

**Martinus Th. van Genuchten, Carolina Naveira-Cotta, Todd H. Skaggs, Amir Raoof, and Elizabeth M. Pontedeiro**

**Abstract** This chapter provides an overview of alternative approaches for modeling water flow and contaminant transport problems in soils and groundwater. Special focus is on flow and transport processes in the variably saturated vadose zone between the soil surface and the groundwater table. The governing flow and transport equations are discussed for both equilibrium and nonequilibrium flow conditions, followed by three examples. The first example shows how one-dimensional root-zone modeling can be used to estimate short- and long-term recharge rates, including contaminant transport through the vadose zone. A second example illustrates a two-dimensional application involving drip irrigation, while the third example deals with two-dimensional nonequilibrium transport of a

M.Th. van Genuchten (✉)
Department of Mechanical Engineering, POLI&COPPE, Universidade Federal do Rio de Janeiro, P.O. Box 68503, Rio de Janeiro, RJ 21945-970, Brazil

Department of Earth Sciences, Utrecht University, Budapestlaan 4, 3584CD Utrecht, The Netherlands
e-mail: rvangenuchten@hotmail.com

C. Naveira-Cotta
Department of Mechanical Engineering, POLI&COPPE, Federal University of Rio de Janeiro, P.O. Box 68503, Rio de Janeiro, RJ 21945-970, Brazil
e-mail: carolina@mecanica.coppe.ufrj.br

T.H. Skaggs
U.S. Salinity Laboratory, USDA-ARS, 450 W. Big Springs Rd., Riverside, CA 92507, USA
e-mail: todd.skaggs@ars.usda.gov

A. Raoof
Department of Earth Sciences, Utrecht University, Budapestlaan 4, 3584CD Utrecht, The Netherlands
e-mail: a.raoof@uu.nl

E.M. Pontedeiro
Department of Nuclear Engineering, POLI&COPPE, Federal University of Rio de Janeiro, P.O. Box 68503, Rio de Janeiro, RJ 21945-970, Brazil
e-mail: bettinadulley@hotmail.com

W.G. Teixeira et al. (eds.), *Application of Soil Physics in Environmental Analyses: Measuring, Modelling and Data Integration*, Progress in Soil Science,
DOI 10.1007/978-3-319-06013-2_15, © Springer International Publishing Switzerland 2014

pesticide in a tile-drained field soil. Also discussed are alternative pore-scale modeling approaches that may provide a better understanding of the basic physical and geochemical processes affecting fluid flow and contaminant transport in saturated and variably saturated media.

**Keywords** Numerical models • Vadose zone • Unsaturated flow • Contaminant transport • HYDRUS • Recharge • Drip irrigation • Pesticide transport • Preferential flow • Pore network models

## 15.1 Introduction

Soil and groundwater contamination by a broad range of agricultural and industrial pollutants is an ever-increasing problem facing this planet. Major sources of both point and non-point source contamination are the use of fertilizers and pesticides in agricultural operations, leaking underground storage tanks, chemical spills, municipal landfills and mine tailings. Specific contaminants include a range of organic and inorganic chemicals such as chlorinated hydrocarbons, phenols, heavy metals, radionuclides, pesticides, nitrates and ammonia, salts, pharmaceuticals and hormones, and many others. Once released into the environment, these contaminants are subject to a large number of often simultaneous physical, chemical, and biological processes, including advective-dispersive transport, sorption-desorption, precipitation-dissolution, volatilization, and biodegradation. Because of these complexities, mathematical models have become critical components of any effort to understand and predict site-specific subsurface water flow and contaminant transport processes. For example, models can be helpful tools for designing, testing and implementing soil, water and crop management practices in agriculture to minimize soil and water contamination by salts, pesticides and toxic trace elements. Models are equally needed for designing or remediating industrial waste disposal sites and landfills, or for long-term stewardship of nuclear waste repositories.

A large number of specialized analytical and numerical models now exist to simulate the various processes at various levels of approximation and for different applications. Modeling approaches range from relatively simple analytical and semi-analytical solutions, to much more complex numerical codes that permit consideration of a large number of simultaneous nonlinear processes. While analytical and semi-analytical solutions undoubtedly remain popular for many applications, especially for solute transport problems (e.g., Vanderborght et al. 2005; van Genuchten et al. 2012; Naveira-Cotta et al. 2013), the development of more versatile and numerically stable solution techniques and the ever-increasing power of personal computers are now facilitating the much wider use of numerical models. The use of numerical models is now also very much facilitated by the availability of specific software packages in both the public and commercial domains, including the development of sophisticated graphical user interfaces that dramatically simplify their use (Šimůnek and Bradford 2008; Mallants et al. 2011). Examples of widely used codes for flow and transport in variably saturated or multiphase systems are MACRO (Jarvis 1994), UNSATCHEM

(Šimůnek et al. 1996), FEHM (Zyvoloski et al. 1997), HYDROBIOGEOCHEM (Yeh et al. 1998), VS2DI (Healy 2008), MODFLOW-SURFACT (Panday and Huyakorn 2008), STOMP (White et al. 2008), SWAP (van Dam et al. 2008), and the HYDRUS (Šimůnek et al. 2008) and TOUGH (Finsterle et al. 2008) family of codes.

In this chapter we give an overview of various approaches for modeling fluid flow and contaminant transport in soils and groundwater. Our focus is especially on transport processes in the vadose zone. We first give a brief overview of the classical flow and transport equations generally used for modeling equilibrium contaminant transport processes in variably saturated media. This includes two applications. One of these considers root-zone modeling to estimate recharge rates in a semi-arid region of Brazil, but also includes downward transport of a contaminant following a chemical spill at the surface. The second example considers a two-dimensional application involving drip irrigation. Next we provide a brief discussion of possible nonequilibrium transport formulations often needed for flow processes in macroporous (structured) soils or unsaturated fractured rock. This includes an example dealing with the two-dimensional nonequilibrium transport of a pesticide in a tile-drained field soil. For our calculations we used the most recent or earlier versions of HYDRUS-1D (Šimůnek et al. 2013) for the one-dimensional problems, and HYDRUS 2/3D (Šimůnek et al. 2012) for the two-dimensional applications. In a separate section we also discuss briefly various pore-scale modeling approaches that may lead a better understanding of the basic physical and biogeochemical processes affecting fluid flow and contaminant transport in saturated and variably saturated media.

## 15.2 Classical Modeling Approaches for Variably Saturated Media

### *15.2.1 Governing Flow and Transport Equations*

Classical descriptions of water and solute movement in the vadose zone are typically based on the Richards equation (Richards 1931) for flow in unsaturated porous media and the advection-dispersion equations for solute transport. Here we present the general equations for variably-saturated multidimensional systems. Water flow in such systems is most often described using the three-dimensional form of the Richards equation as follows

$$\frac{\partial \theta(h)}{\partial t} = \frac{\partial}{\partial x_i}\left[K\left(K_{ij}^A \frac{\partial h}{\partial x_j} + K_{ij}^A\right)\right] - S_w \tag{15.1}$$

in which $\theta$ is the volumetric water content, $h$ is the soil water pressure head, $x_i$ ($i = 1,2,3$) are the spatial coordinates, $t$ is time, $S_w$ is a general source/sink term (often used to account for water uptake by plant roots), $K_{ij}^A$ are components of a

dimensionless anisotropy tensor, and $K$ is the unsaturated hydraulic conductivity function given by

$$K(h;x,y,z) = K_s(x,y,z)K_r(h;x,y,z) \tag{15.2}$$

where $K_r$ is the relative hydraulic conductivity ($0 \leq K_r \leq 1$), and $K_s$ the saturated hydraulic conductivity. The anisotropy vector ${K_{ij}}^A$ may be used to account for anisotropic media. For an isotropic medium, the diagonal entries of ${K_{ij}}^A$ are equal to one and the off-diagonal entries zero. If Eq. 15.1 is used for flow in a vertical cross-section, $x_1 = x$ is the horizontal coordinate, and $x_2 = z$ is the vertical coordinate of the medium, the latter being directed positive upward.

Contaminant transport can be described similarly using the general advection-dispersion equation. Ignoring any partitioning into to the gas phase, the general equation is given by

$$\frac{\partial(\theta c)}{\partial t} + \frac{\partial(\rho s)}{\partial t} = \frac{\partial}{\partial x_i}\left(\theta D_{ij}\frac{\partial c}{\partial x_j}\right) - \frac{\partial q_i c}{\partial x_i} - S_s \tag{15.3}$$

where $c$ and $s$ are solute concentrations associated with the liquid and solid phases, respectively, $S_s$ is a general source-sink term, and $q_i$ is the volumetric fluid flux given by Darcy-Buckingham's law as (Narasimhan 2005)

$$q_i = -K\left(K_{ij}^A\frac{\partial h}{\partial x_I} + K_{ij}^A\right) \tag{15.4}$$

while $D_{ij}$ represents the dispersion coefficient tensor, generally assumed to be of the form (e.g., Bear 1972)

$$\theta D_{ij} = \theta D_o \tau \delta_{ij} + (D_L - D_T)\frac{q_i q_j}{|q|} + D_T|q|\delta_{ij} \tag{15.5}$$

in which $D_o$ is the ionic or molecular diffusion coefficient, $\tau$ is a water content dependent tortuosity factor (e.g., Millington and Quirk 1961), $\delta_{ij}$ is the Kronecker delta function ($\delta_{ij} = 1$ if $i = j$, and $\delta_{ij} = 0$, if $i \neq j$), and $D_L$ and $D_T$ are the longitudinal and transverse dispersivities, respectively.

The above equations are for water flow and contaminant transport. Many applications may further include heat transport. The governing equation is then of the form (e.g., Šimůnek et al. 2012)

$$C_p(\theta)\frac{\partial T}{\partial t} = \frac{\partial}{\partial x_i}\left(\lambda_{ij}\frac{\partial T}{\partial x_j}\right) - C_w q_i\frac{\partial T}{\partial x_{is}} - S_T \tag{15.6}$$

where $T$ is temperature, $C_p$ and $C_w$ are volumetric heat capacities of the porous medium and the liquid phase, respectively, $S_T$ is a general source-sink term, and $\lambda_{ij}$ is the apparent thermal conductivity of the soil given by

$$\lambda_{ij}(\theta) = \lambda_o(\theta)\delta_{ij} + (\lambda_L - \lambda_T)\frac{q_i q_j}{|q|} + \lambda_T C_w |q| \delta_{ij} \tag{15.7}$$

in which $\lambda_o$ is a thermal conductivity accounting for the tortuosity of the porous medium, and $\lambda_L$ and $\lambda_T$ are the longitudinal and transverse thermal dispersivities, respectively. We refer to the HYDRUS 2/3D technical manual (Šimůnek et al. 2012) for a more detailed discussion of the above equations for water, solute and heat movement.

Applications of the above equations require definition of problem-specific initial and boundary conditions. A large number of boundary conditions are available for this purpose, including transient atmospheric conditions as explained by Šimůnek et al. (2012). Several of these conditions are discussed later in this chapter as part of the applications. Also needed is information about the unsaturated hydraulic functions. A number of specific models are available for this purpose (e.g., Brooks and Corey 1964; van Genuchten 1980; Durner 1994; Kosugi 1996; and many others), as summarized well in a study by Leij et al. (1997).

### 15.2.2 One-Dimensional Application to Recharge

Here we use the classical models to illustrate water flow and solute transport processes in a 8-m deep one-dimensional soil profile, with special attention to root water uptake and estimating recharge using time-dependent atmospheric boundary conditions. The governing flow Eq. 15.1 for this problem reduces then to

$$\frac{\partial \theta(h)}{\partial t} = \frac{\partial}{\partial z}\left(K(h)\frac{\partial h}{\partial z} + K(h)\right) - S_w \tag{15.8}$$

The soil hydraulic (constitutive) relationships needed in applications of Eqs. 15.1 and 15.8 are described here using the functions (van Genuchten 1980)

$$\theta(h) = \theta_r + \frac{\theta_s - \theta_r}{\left[1 + |\alpha h|^n\right]^m} \qquad (m = 1 - 1/n) \tag{15.9}$$

$$K(h) = K_s S_e^l \left[1 - \left(1 - S_e^{1/m}\right)^m\right]^2 \tag{15.10}$$

where $\theta_r$ and $\theta_s$ denote the residual and saturated water contents, respectively, $\alpha$ and $n$ are empirical shape factors, $K_s$ is the saturated hydraulic conductivity, $l$ is a pore-connectivity parameter, and $S_e$ is effective saturation given by

$$S_e(h) = \frac{\theta - \theta_r}{\theta_s - \theta_r} \tag{15.11}$$

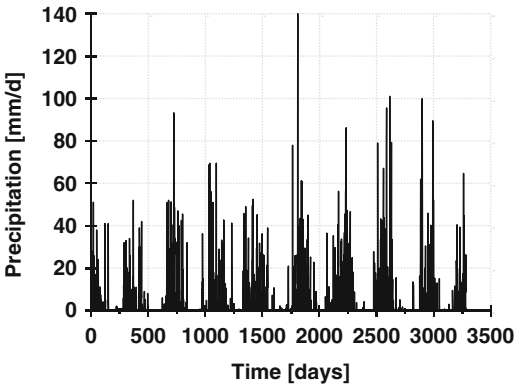


**Fig. 15.1** Daily rainfall rates used for the recharge example

For our example, Fig. 15.1 shows the rainfall pattern we used, typical of a semi-arid region of Minas Gerais State in the Cerrado area of Brazil. Much of the rainfall occurs in the Brazilian summer months (January-March), while the winters are relatively dry. The example was selected to show many of the features involved in water flow through the vadose zone, including water uptake by plant roots and evaluating deep drainage and recharge. Root zone modeling has become a popular approach for estimating recharge (Jimenez-Martinez et al. 2009; Lu et al. 2011; Assefa and Woodbury 2013), among many other approaches (Gee and Hillel 1988; Scanlon et al. 2002). For the recharge calculations using HYDRUS-1D (Šimůnek et al. 2012) we assumed a one-dimensional vertical profile of 8 m. Atmospheric boundary conditions were assigned to the soil surface with the possibility of runoff. Daily values of precipitation and potential evapotranspiration were used, in combination with the water stress response model of Feddes et al. (1978) to account for root water uptake by the grass cover.

Daily potential evapotranspiration rates were calculated using the approach of Hargreaves (Hargreaves 1975; Jensen et al. 1990) which is considered one of the best when limited weather data are available. The method uses daily minimum and maximum temperature data, the latitude and altitude of the site, the leaf area index of the vegetative cover (2.0 in our example), and the rooting depth (70 cm). HYDRUS-1D default parameter values for the water stress response function of Feddes et al. (1978) were used in this hypothetical example. We further assumed a linearly decreasing root distribution from the soil surface (maximum) to a depth of 70 cm. Soil hydraulic parameters were estimated from available soil texture data of the site using the pedotransfer functions of Schaap et al. (2001) as implemented in HYDRUS-1D.

Several alternatives were considered for the initial and lower boundary conditions. One set of calculations simply assumed a constant initial condition of $-150$ cm versus depth, which is close to the long-term average pressure head distribution found with the calculations, along with a free-draining soil profile (represented by the condition that $\partial h/\partial z$ at the lower boundary is zero) which neglects the presence of a water table.

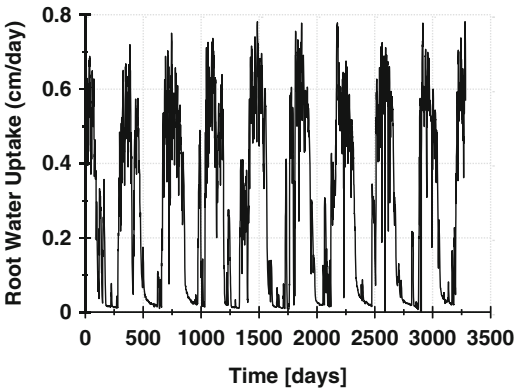


**Fig. 15.2** Calculated root water uptake rates for the recharge example

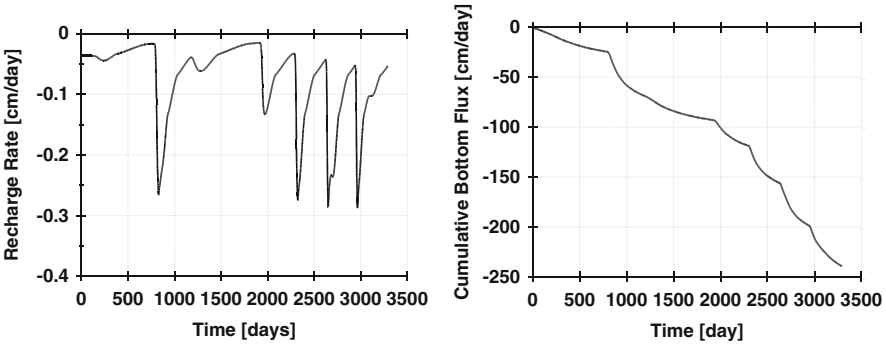


**Fig. 15.3** Calculated instantaneous (*left*) and cumulative (*right*) recharge rates

Figure 15.2 shows the calculated root water uptake during the 9 years of simulation, while the calculated recharge rate for the free-draining profile is plotted in Fig. 15.3. Figure 15.3 further shows the calculated cumulative recharge rate (the cumulative bottom flux from the 8-m deep profile). The recharge rate in Fig. 15.3 and the root water uptake rate in Fig. 15.2 show close correlation with the precipitation data in Fig. 15.1, with the recharge rate being highest shortly after the maximum precipitation rates occur in the winter months. The average recharge rate during the 9 years was approximately 270 mm/year (best calculated as the average slope versus time of the cumulative bottom flux shown in Fig. 15.3).

The results in Fig. 15.3 were obtained assuming that the recharge rate does not depend on transient changes in the phreatic surface, including the upward/downward movement of the capillary fringe due to regional flow effects or time-dependent weather conditions. One alternative boundary condition would be the use of a transient condition specifying the water table consistent with local measurements, or perhaps even considering the presence of a constant water table. The latter case was considered by fixing a permanent water table at the bottom boundary. The calculated recharge rates in that case remained very close to those in Fig. 15.2, except that the peaks occurred slightly earlier.

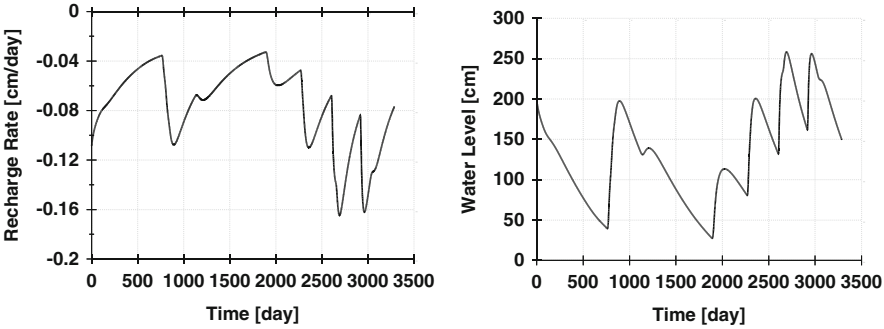


**Fig. 15.4** Calculated recharge rates (*left*) and position of the water table (above the *bottom* boundary of the flow domain at a depth of 800 cm) for the recharge example

We further experimented with a special deep drainage lower boundary condition available within HYDRUS-1D to account in an approximate way for regional flow effects on the recharge rate. This boundary is given by (Hopmans and Stricker 1989):

$$q_L(t) = A \exp\left[-B\left|h_L - h_{gw}\right|\right] \tag{15.12}$$

where $q_L$ is the imposed lower boundary flux, $h_L$ is the transient pressure head at the lower boundary (to be calculated), $A$ and $B$ are adjustable parameters, and $h_{gw}$ is some long-term equilibrium water table position relative to the lower boundary. The three parameters ($A$, $B$ and $h_{gw}$) are essentially empirical. Their values in this example were guided by water table data of the Rio Claro Aquifer as observed in monitoring wells drilled on the Rio Claro campus of São Paulo State University in Rio Claro, SP, Brazil (Neto et al. 2014).

The initial condition for the deep drainage condition was taken to be −150 cm within the upper part of the profile, the same as before, but now with a pressure head distribution in the lower part of the profile that is in equilibrium with the water table at 600 cm depth. The initial pressure head at the lower boundary of the 8-m deep profile hence was 200 cm. Figure 15.4 shows the calculated recharge rates for the deep drainage boundary condition. Results were obtained using values for $A$, $B$ and $h_{gw}$ of −2.5 cm/day, −0.007 $cm^{-1}$ and 600 cm, respectively. As compared to the plot in Fig. 15.2, the recharge rate is now less variable in time since the net rate also includes the upward (during the rainy winter seasons) and downward (the summer seasons) movement of the capillary fringe. The upward and downward movement of the water table as such moderated the local fluid fluxes close to the water table and within the capillary fringe. However, the downward fluxes in the vadose zone above the capillary fringe were affected only minimally. Also, the overall cumulative (recharge) fluxes through the lower boundary during the 9-year simulation for the two boundary conditions were relatively close: 239 versus 253 during 9 years (26.6 versus 28.1 cm/year) for the free drainage and deep drainage conditions, respectively.

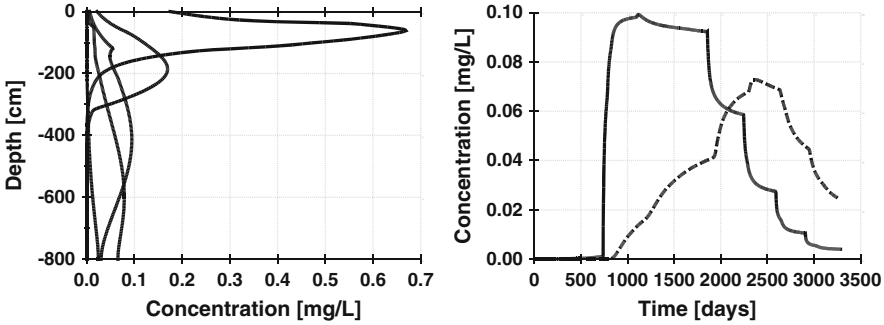


**Fig. 15.5** Calculated concentration distributions versus depth 1, 2, 4, 6 and 9 years after a 1 cm chemical spill (*left*) and concentrations versus time at two observation nodes (*right*) located at depths of 4 m (*solid line*) and 8 m (*dashed line*) for the free drainage scenario

Figure 15.4 also shows the transients of the calculated water table position (in terms of the simulated pressure heads above the lower boundary at 800 cm below the soil surface). Results indicate an oscillating water table, very much in response to the local precipitation, potential evapotranspiration and root water uptake conditions.

Finally, we also used the recharge example to estimate the transport of a contaminant at the site, assuming that on day 1 a 1-cm spill occurred of a nonreactive pollutant having a concentration of 20 mg/L. Simulations assumed applicability of the equilibrium transport model given by Eq. 15.2, which for the current one-dimensional scenario reduces to the relatively simple

$$\frac{\partial(\theta c)}{\partial t} = \frac{\partial}{\partial z}\left(\theta D \frac{\partial c}{\partial z}\right) - \frac{\partial qc}{\partial z} \tag{15.13}$$

where $q$ is the Darcy-Buckingham fluid flux given by

$$q = -K(h)\frac{\partial h}{\partial z} - K(h) \tag{15.14}$$

and $D$ is the dispersion coefficient given by

$$D = D_o\tau + D_L\frac{|q|}{\theta} \tag{15.15}$$

in which $D_o$ is the diffusion coefficient of the contaminant (1 $cm^2$/day in our example), and $D_L$ the longitudinal dispersivity (assumed to be 40 cm). Equation 15.13 holds for the relatively simple case of no contaminant sorption onto the solid phase of the soil (an inert tracer), and no partitioning of the contaminant into the air phase.

Figure 15.5 shows calculated concentration distributions versus depth, 1, 2, 4, 6 and 9 years after the 1-cm chemical spill (left), and concentrations versus time at

two observation nodes located at depths of 4 and 8 m deep (right) for the free drainage example. Notice that the contaminant front reached the bottom of the profile after about 1,000 days, and that the maximum concentration of the solute pulse decreased from 20 mg/L (the concentration of the 1 cm spill) to about 0.07 mg/L at 8 m depth, mostly because of dilution with initially present water and infiltrating rain water. Results for the deep drainage bottom boundary were essentially identical in the upper part of the profile (e.g., the distribution versus time at 4 m in Fig. 15.5 was exactly the same), and deviated only minimally in the lower part of the profile because of some additional mixing with transient changes of the capillary fringe and the groundwater table.

The above example was selected to show a number of features that can be captured relatively easily in numerical solutions of the governing flow and transport equations, in this case infiltration, root water uptake, deep drainage and recharge, and contaminant transport. All calculations were carried out using HYDRUS-1D, which can be downloaded freely from www.pc-progress.com. Other features included in HYDRUS-1D, not further discussed here, are such processes as linear and nonlinear sorption, physical and chemical nonequilibrium transport, multicomponent transport, and virus and colloid transport, including consideration of both direct (forward) and inverse (parameter estimation) problems. Several examples for multicomponent transport are provided by Šimůnek et al. (2014, this issue).

### *15.2.3 Two-Dimensional Application to Subsurface Drip Irrigation*

This example considers a typical agricultural problem in which irrigation water is applied to a two-dimensional soil profile using subsurface drip irrigation (Fig. 15.6). Drip irrigation has become a popular method for improving water use efficiency in agricultural operations, especially in arid and semi-arid areas (Skaggs et al. 2004; Lazarovitch et al. 2005; Hanson et al. 2008; Kandelous et al. 2011; Rodriguez-Sinobas et al. 2012). Advantages are improved management of water, soil salinity, fertilizers and pesticides, including through fertigation practices in which agricultural chemicals are supplied directly with the applied irrigation water to the root zone of crops.

Figure 15.6 shows the finite element grid used for one set of simulations documented in more detail by Skaggs et al. (2004). The simulated right side of the profile consisted of a 60 cm wide, 70 cm deep cross-section, with a dripper represented by a half-circle along the left side of the domain 6 cm below the soil surface. Water was applied at a constant rate of 6.37 cm/h through the drip tubing boundary, equivalent to a constant water flux of 4 L/h per m drip tubing. The left, right and soil surface boundaries were assumed to be no-flow boundaries, thereby assuming that evaporation and drainage were negligible during the considered

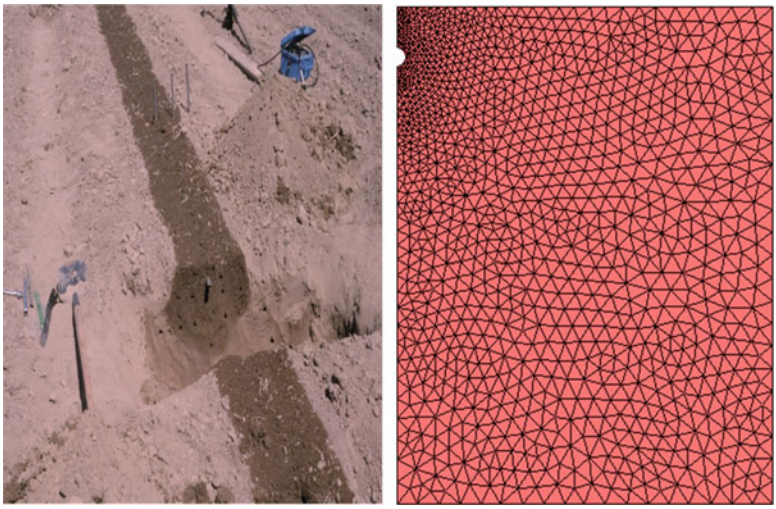

**Fig. 15.6** Picture of the simulated drip irrigation experiment (*left*) in the San Joaquin Valley of California as documented by Skaggs et al. (2004), and the invoked finite element grid used for the simulations (*right*). Because of symmetry, only half of the cross-section was considered

irrigation and water redistribution times. A free drainage condition was applied to the lower boundary. Simulations were carried out using hydraulic parameters in Eqs. 15.9 and 15.10 estimated using pedotransfer functions developed by Schaap et al. (2001) leading to the following values: $\theta_r = 0.021$, $\theta_s = 0.34$, $\alpha = 0.023$ cm$^{-1}$, $n = 1.4$, $K_s = 1.6$ cm/h, and $l = -0.92$.

Figure 15.7 shows the measured and simulated water content contour plots for one of the experiments by Skaggs et al. (2004). The irrigation rate for this example was 40 L per m of tubing. The figure shows excellent agreement between the measured and simulated water contents, with root-mean-square errors (RMSEs) being 0.027 and 0.013 cm$^3$ cm$^{-3}$ at times of 10.75 h (45 min after the 10-h irrigation), and 31 h following an extended period of redistribution. The relatively close fit of simulated and measured values was due in part to having a relatively precise prediction of the hydraulic properties using soil texture data as well as measured values of the water contents at 330 and 15,000 cm as required by the most general option in Rosetta (Schaap et al. 2001). Equally important, the simulation involved a scenario where the irrigation rate is known, thus involving flux-controlled infiltration in which the simulated and calculated total infiltration rates must be the same. More deviations are expected for profile-controlled irrigation scenarios, such as during ponding of a soil surface or, as could be possible with the present example, when a relatively high flux is given such that saturated conditions near the dripper may develop. This may lead to a back pressure that could significantly reduce the drip discharge rate (e.g., Lazarovitch et al. 2005).

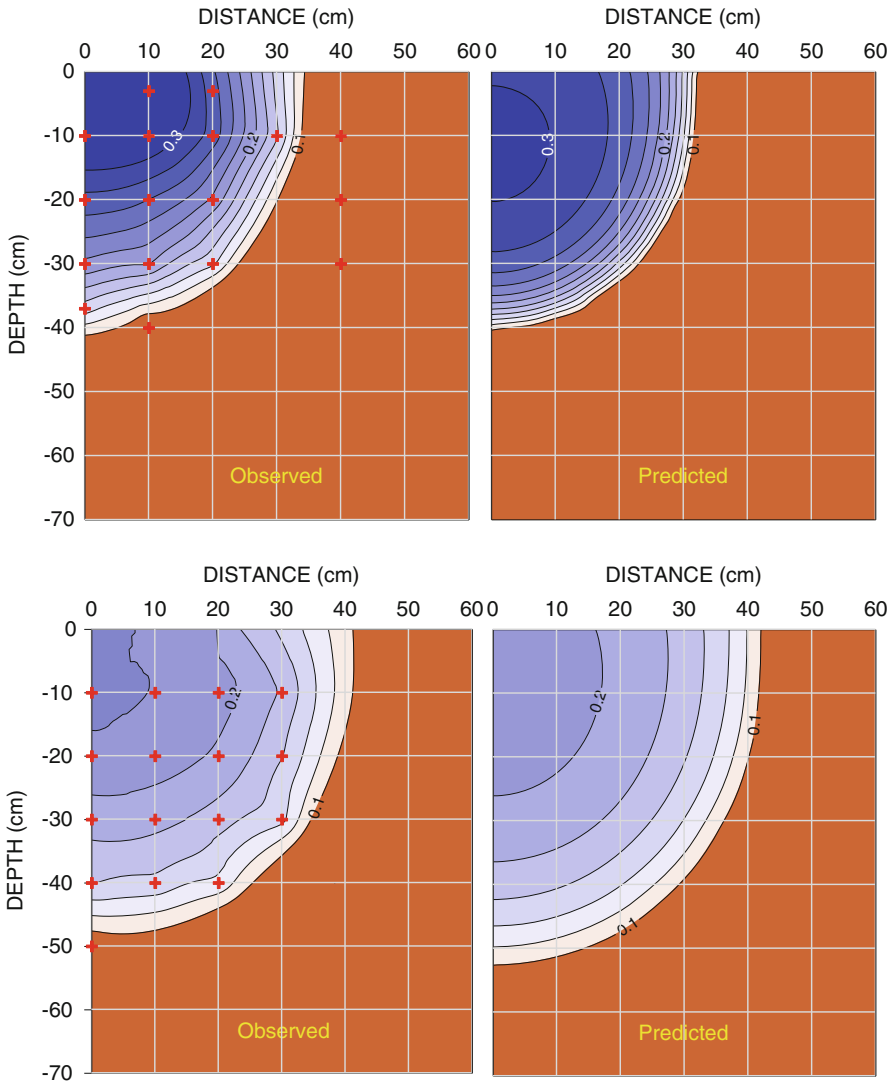


**Fig. 15.7** Measured and calculated volumetric water content contours for a 10 h long, 40 L/m subsurface drip irrigation experiment. Plots are for times $t = 10.75$ h (45 min after the 10 h irrigation terminated; *top* plots), and $t = 31$ h (after 21 h of redistribution; *bottom* plots)

The above drip irrigation example showed very good agreement between measured and predicted water content distributions. As indicated by Skaggs et al. (2004), the results provide support for using numerical models such as HYDRUS 2/3D as a tool for investigating and designing drip irrigation management practices. This may include estimating optimal depths and spacing of the drip irrigation line as a function of soil texture, emitter discharge, initial water content, irrigation frequency and crop rooting patterns (e.g. Skaggs et al. 2010).

## 15.3 Nonequilibrium Model Formulations

The various model descriptions thus far involved very classical descriptions of water flow and solute transport assuming equilibrium conditions. Much evidence exists that water and solutes in many or most field soils do not move according to the uniform flow pattern typically predicted with the Richards equations and the advection-dispersion equations (Hendrickx and Flury 2001; Jarvis 2007; Gerke et al. 2010). This is due to the presence of macropores, fractures or other structural voids or biological channels through which water and contaminants may move preferentially, thereby bypassing parts of the matrix pore-space. Unstable flow in homogeneous or heterogeneous soil, hydrophobicity and the presence of sloping soil textural layers often also contribute to this apparent larger-scale non-equilibrium situation. The resulting nonequilibrium or preferential flow processes seriously hamper accurate predictions of contaminant transport in soils and fractured rocks (Šimůnek et al. 2003; Gerke 2006; Gerke et al. 2010). Contrary to uniform flow, preferential flow results in irregular wetting of the soil profile as a direct consequence of water moving faster in certain parts of the soil profile than in others. Water and dissolved contaminants for these reasons can move quickly to far greater depths, and much faster, than would be predicted with the Richards equation describing uniform flow.

### *15.3.1 Governing Equations*

Nonequilibrium or preferential flow in macroporous soils and fractured rocks can be described using a variety of dual-porosity and dual-permeability models (Liu 1998; Šimůnek et al. 2003; Gerke 2006; Larsbo et al. 2005; Köhne et al. 2009; Vogel et al. 2010). Figure 15.8 shows a schematic of possible equilibrium and

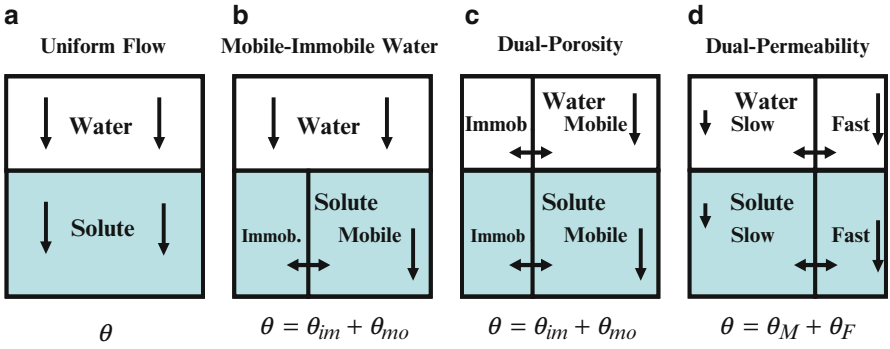


**Fig. 15.8** Conceptual models for equilibrium and preferential flow of water and solutes. In the figure, $\theta$ is the water content, $\theta_{mo}$ and $\theta_{im}$ in (b) and (c) are water contents of the mobile and immobile flow regions, respectively, $\theta_M$ and $\theta_F$ in (d) are water contents of the matrix and macropore (fracture) regions, respectively, and $c$ are concentrations of corresponding regions, with subscripts having the same meaning as for the water contents (After Šimůnek and van Genuchten 2008)

physical nonequilibrium models for water flow and solute transport (Šimůnek and van Genuchten 2008). The nonequilibrium models typically assume that the porous medium consists of two interacting pore regions, one associated with the inter-aggregate, macropore, or fracture system, and one comprising the micropores (or intra-aggregate pores) inside soil aggregates or the rock matrix. Dual-porosity models assume that water in the matrix is stagnant, while the more complex dual-permeability models allow transient water flow to occur also within the soil or rock matrix.

In the dual-permeability approach, Richards equations are applied to both the macropore or fracture (subscript $f$) and matrix regions (subscript $m$) as represented by the schematic in Fig. 15.8. For one-dimensional systems, the flow equations for the fracture and matrix regions are given by

$$\frac{\partial \theta_f(h_f)}{\partial t} = \frac{\partial}{\partial z}\left[K_f(h_f)\,\frac{\partial h_f}{\partial z} - K(h_f)\right] - \frac{\Gamma_w}{w} \tag{15.16a}$$

$$\frac{\partial \theta_m(h_m)}{\partial t} = \frac{\partial}{\partial z}\left[K_m(h_m)\,\frac{\partial h_m}{\partial z} - K_m(h_m)\right] + \frac{\Gamma_w}{1-w} \tag{15.16b}$$

respectively, where $w$ is the ratio of the volumes of the fracture domain and the total soil system, and $\Gamma_w$ is the transfer term for fluid exchange between the two regions. The mobile and immobile water contents $\theta_{mo}$ and $\theta_{im}$ in Fig. 15.8 are related to the local fracture and matric water contents $\theta_f$ and $\theta_m$ in Eqs. 15.16a and 15.16b through $\theta_{mo} = w\theta_f$ and $\theta_{im} = (1\text{-}w)\theta_m$, respectively.

Different dual-permeability formulations arise depending upon how water and/or solute movement in the micropore region is modeled, and how water and solutes in the fracture and matrix regions are allowed to interact through the exchange term $\Gamma_w$ (Šimůnek et al. 2003; Larsbo et al. 2005). One approach is to use a first-order driving force in the pressure head as follows (Gerke and van Genuchten 1993):

$$\Gamma_w = \alpha_w(h_f - h_m) \tag{15.17}$$

in which $\alpha_w$ is a first-order mass transfer coefficient of the form:

$$\alpha_w = \frac{\beta \gamma_w K_a(h)}{a^2} \tag{15.18}$$

where $\beta$ is a dimensionless geometry-dependent coefficient, $a$ is the characteristic length of the matrix structure (e.g., half of the fracture spacing or the radius of spherical aggregates), $\gamma_w$ is a dimensionless scaling coefficient, and $K_a$ is the effective hydraulic conductivity of the fracture-matrix interface, which may not be the same as the matrix conductivity because of fracture coatings. Various expressions for $K_a(h)$ have been used in the literature (Zimmerman et al. 1993; Gerke and van Genuchten 1996; Köhne et al. 2004).

Analogous to Eqs. 15.16a and 15.16b, the dual-permeability formulation for solute transport is based on advection-dispersion type equations for transport in both the fracture and matrix regions as follows (Gerke and van Genuchten 1993):

$$\frac{\partial \theta_f R_f c_f}{\partial t} = \frac{\partial}{\partial z}\left(\theta_f D_f \frac{\partial c_f}{\partial z}\right) - \frac{\partial q_f c_f}{\partial z} - \phi_f - \frac{\Gamma_s}{w} \tag{15.19a}$$

$$\frac{\partial \theta_m R_m c_m}{\partial t} = \frac{\partial}{\partial z}\left(\theta_m D_m \frac{\partial c_m}{\partial z}\right) - \frac{\partial q_m c_m}{\partial z} - \phi_m + \frac{\Gamma_s}{1-w} \tag{15.19b}$$

where as before the subscripts $f$ and $m$ refer to the fracture and matrix pore regions, respectively, and $\Gamma_s$ is the mass transfer term for solute exchange between the two regions. The latter includes both diffusional exchange as well as advective mass transport between the fracture and matrix regions.

The above dual-permeability formulation presents a potentially very powerful model for simulating preferential flow and transport processes in the subsurface as shown by several recent examples in the literature (Pot al. 2005; Kodesova et al. 2005; Köhne et al. 2006; Vogel et al. 2010; among others). While relatively complicated mathematically, the complexity is merely a reflection of the complicated nature in which preferential flow occurs, and the many physical and chemical processes and parameters involved. Unfortunately, application of dual-permeability models such as Eqs. 15.16a and 15.16b typically requires two water retention functions, one for the matrix and one for the fracture pore system, and two or three hydraulic conductivity functions: $K_f(h_f)$ for the fracture network, $K_m(h_m)$ for the matrix, and possibly a separate conductivity function $K_a(h_a)$ for the fracture/matrix interface as embedded in the exchange term, $\Gamma_w$ (Gerke and van Genuchten 1993). Such information is not readily available for most practical applications. For these reasons a number of simplifications are often invoked, such as the use of dual-porosity formulations, exemplified by the schematic of Fig. 15.8c, which still allow exchange between the fracture and matrix regions, but assume that no longitudual flow and transport occurs within the matrix domain.

To avoid over-parameterization of the governing equations, a further simplification is possible by assuming instantaneous hydraulic equilibration between the fracture and matrix region during flow such that $h_f = h_m$ $(=h)$. In that case the coupling term $\Gamma_w$ can be eliminated from Eqs. 15.16a and 15.16b to recover Eq. 15.1, but now with composite hydraulic properties of the form

$$\theta(h) = w\theta_f(h) + (1-w)\theta_m(h) \tag{15.20a}$$

$$K(h) = wK_f(h) + (1-w)K_m(h) \tag{15.20b}$$

While still leading to uniform flow, models using such composite hydraulic properties do allow for enhanced flow during conditions near saturation, and as such may provide more realistic simulations of field data than the standard Richards equation with unimodal hydraulic properties (Peters and Klavetter 1988; Mohanty et al. 1997; Zurmühl and Durner 1996; Schaap and van Genuchten 2006). For example, the hydraulic functions of Vogel et al. (2000) are given by

$$\theta(h) = \begin{cases} \theta_r + \dfrac{\theta_m - \theta_r}{\left(1 + |\alpha h|^n\right)^m} & h < h_s \\ \theta_s & h \geq h_s \end{cases} \tag{15.21}$$

$$K(h) = \begin{cases} K_k \left(\dfrac{\theta - \theta_r}{\theta_k - \theta_r}\right)^l \left[\dfrac{1 - F(\theta)}{1 - F(\theta_k)}\right]^2 & h \leq h_k \\ K_k + \dfrac{(h - h_k)(K_s - K_k)}{h_s - h_k} & h_k < h < h_s \\ K_s & h \geq h_s \end{cases} \tag{15.22}$$

where

$$F(\theta) = \left[1 - \left(\frac{\theta - \theta_r}{\theta_m - \theta_r}\right)^{1/m}\right]^m \tag{15.23}$$

Equation 15.21 introduces a very small but non-zero air entry value in $\theta(h)$ near saturation by replacing $\theta_s$ in Eq. 15.5 with by an extrapolated parameter $\theta_m$ slightly larger than $\theta_s$. While this modification has little or no effect on the retention curve, the effect on the shape and value of the hydraulic conductivity function can be considerable for fine-textured soils (Vogel et al. 2000; Schaap and van Genuchten 2006). Equation 15.22 assumes that the predicted hydraulic conductivity function is matched to a measured value of the conductivity, $K_k = K(\theta_k)$, at some water content, $\theta_k \leq \theta_s$ and $K_k \leq K_s$. The conductivity function is then assumed to increase linearly between $h_k$ and saturation to account for macropore flow.

When the Richards equation Eq. 15.1 is used in conjunction with composite (dual-porosity) hydraulic functions such as Eqs. 15.20a and 15.20b or 15.21 and 15.22, the solute transport model reduces to a relatively standard dual-porosity formulation which assumes that the liquid phase can be partitioned into mobile, $\theta_{mo} = w\theta_f$, and immobile, $\theta_{im} = (1\text{-}w)\theta_f$, regions, with advective-dispersive transport being restricted to the mobile region as follows (van Genuchten and Wagenet 1989):

$$\frac{\partial \theta_{mo} R_{mo} c_{mo}}{\partial t} = \frac{\partial}{\partial z}\left(\theta D \frac{\partial c_m}{\partial z}\right) - \frac{\partial q c_m}{\partial x} - \alpha_s (c_m - c_{im}) - \phi_{mo} \tag{15.24a}$$

$$\frac{\partial \theta_{im} R_{im} c_{im}}{\partial t} = \alpha_s (c_{mo} - c_{im}) - \phi_{im} \tag{15.24b}$$

in which

$$R_{mo} = 1 + \frac{f \rho K_d}{\theta_{mo}} \qquad R_{mo} = 1 + \frac{(1 - f)\rho K_d}{\theta_{im}} \tag{15.25}$$

where the subscripts *mo* and *im* refer to the mobile (fracture) and immobile (matrix) regions, respectively (Fig. 15.8), $f$ is the dimensionless fraction of sorption sites in

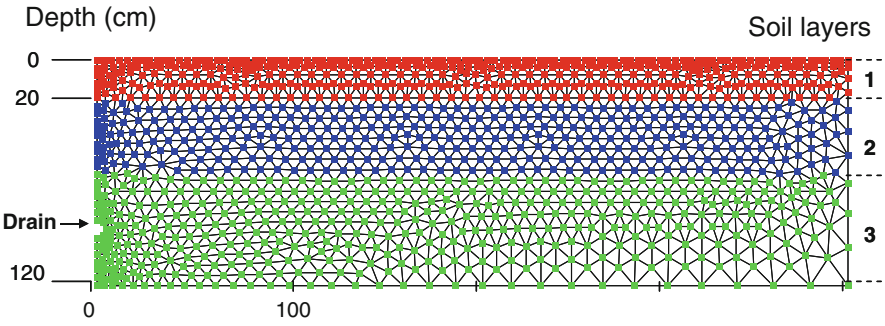


**Fig. 15.9** Unstructured finite element grid used for the layered transport domain representing half the drain spacing of the modeled Bouzule-2 silty clay site. The grid consisted of 2,298 triangular elements and 1,237 nodes

contact with mobile water, $\alpha_s$ is the solute mass transfer coefficient between the two regions, and $K_d$ is the distribution coefficient for linear sorption. Please note that the mass transfer terms in Eqs. 15.24a and 15.24b do not contain the mobile water content, $\theta_{mo}$, such as was the case with Eqs. 15.19a and 15.19b. This was done to keep the same notation as used previously by van Genuchten and Wierenga (1976) and van Genuchten and Wagenet (1989).

### *15.3.2 Application to Field-Scale Pesticide Transport*

We now briefly show one application of the physical nonequilibrium model consisting of the standard Richards equation for water flow in conjunction with composite hydraulic functions (in this example given by Eqs. 15.21 and 15.22, and the dual-porosity model for solute transport Eqs. 15.24a and 15.24b. The example concerns the subsurface transport of the herbicide bentazone in a tile-drained agricultural field in northeastern France (Boivin et al. 2006). The field site (La - Bouzule-2) consisted of relatively fine-textured silty clay. The site was equipped with a subsurface tile drain system (0.05 m diameter), with tiles at an average depth of 0.9 m and a drain spacing of 8 m. Precipitation rates and other meteorological variables were recorded at a weather station close to the site. Bentazone was sprayed on the field on March 11, 2002. We used HYDRUS to simulate two-dimensional variably-saturated flow and pesticide transport. The governing equations are exactly the same Eqs. 15.24a and 15.24b as before, except for their extension to two dimensions (Boivin et al. 2006). For the study we assumed isotropic media, included provisions for root water uptake, but neglected pesticide degradation since laboratory experiments indicated little or no degradation over time periods pertinent to the field experiments. We refer to Boivin et al. (2006) for a detailed discussion of the experiments and the data used for the simulations.

Figure 15.9 shows a cross-section of the simulated domain with the unstructured finite element grid used in the simulations. The grid was stratified in accordance

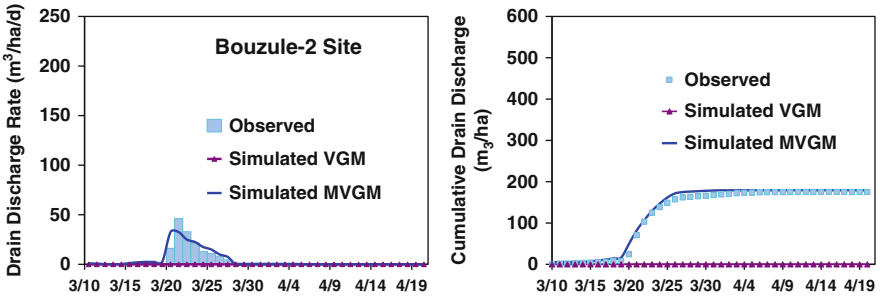


**Fig. 15.10** Observed and simulated instantaneous and cumulative tile drain discharge rates

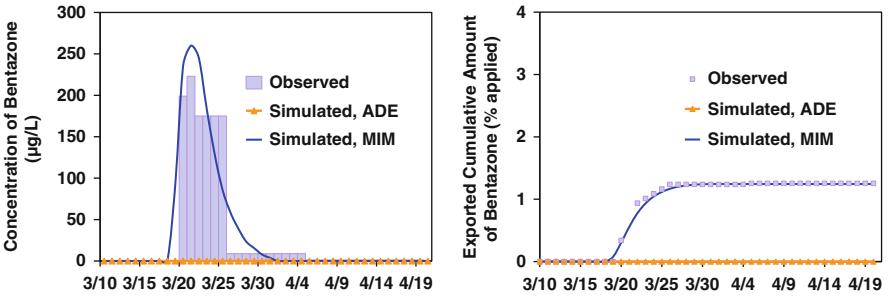


**Fig. 15.11** Observed and simulated bentazone concentrations in the drainage water (*left*) and cumulative amount of bentazone exported (*right*) for the Bouzule-2 silty clay site. Solute transport simulations were carried out with both the advection-dispersion equation (ADE) and the mobile-immobile non-equilibrium transport model (MIM)

with observed soil profile layering. Boundary conditions included no-flow boundaries on the sides, atmospheric conditions at the soil surface (daily precipitation and evaporation rates), a free drainage condition bottom boundary, and a seepage face along the tile drain (which implies that the drain functions only when the surrounding soil is saturated). Preliminary simulations started on January 10, 2002, about 2 months before the pesticide application, with an equilibrium pressure head profile so as to obtain realistic soil water contents in the profile at the time of the pesticide application.

Observed and measured tile drainage discharge rates and concentrations, as well as cumulative amounts, are shown in Figs. 15.10 and 15.11. Observed concentration data (Fig. 15.11) indicated very high pesticide concentrations in the drainage water (a maximum concentration of 223 µg $L^{-1}$), substantially higher than the limit of 0.1 µg $L^{-1}$ set by the European Union for pesticide concentrations in groundwater (FLMW 1995), and also well above 3 µg $L^{-1}$ used by the U.S. Environmental Protection Agency for the maximum contaminant level for bentazone (USEPA 2004). Evidence of preferential flow at this site was clearly demonstrated by several other experiments conducted with a bromide tracer and the pesticide metolachlor in drainage water, especially during the relatively wet spring and summer seasons (Novak et al. 2003).

Two-dimensional HYDRUS simulations using the traditional van Genuchten-Mualem (VGM) hydraulic functions given by Eqs. 15.9 and 15.10 were found to severely underestimate the observed drain discharge rates (Fig. 15.10). $K_s$ values obtained from laboratory experiments did not account for the influence of cracks, and thus substantially underestimated actual $K_s$ values in the field, especially in the spring and summer months when drying cracks were known to develop in especially the soil surface horizon. To account for these cracks, the modified (MVGM) soil hydraulic functions of Vogel et al. (2000) were used to mimic preferential flow of water and solute.

Using Eqs. 15.21 and 15.22 with $K_s$ values up to about 20 times the measured $K_k$ values for some of the layers did lead to much more accurate simulations of the drain discharge rate during the spring of 2002. It is very unlikely that the selected combination of $K_k$ values in the simulations represented a single unique description of the macropore flow processes at the site. Only a few hydraulic parameters in Eqs. 15.21 and 15.22 were obtained from direct measurements (notably $\theta_s$, $\theta_s$ and $K_k$). Others ($\alpha$ and $n$) were estimated from soil texture using the Rosetta pedotransfer functions of Schaap et al. (2001), while $K_s$ and $h_k$ were calibrated against the observed drainage data.

Figure 15.11 shows that the concentrations and amounts of leached pesticide were severely underestimated using the equilibrium (ADE) model. An excellent fit could be obtained with the physical nonequilibrium mobile-immobile (MIM) model upon calibration of the mass transfer coefficient, $\alpha_s$, and equating the immobile water content, $\theta_{im}$, to the residual water content, $\theta_r$ for all three layers. A single $\alpha_s$ value of 0.027 $d^{-1}$ for all three layers produced excellent agreement with the measured concentrations as (Fig. 15.11) as well as the total amount of bentazone exported with the drainage water. The fitted value of 0.027 $d^{-1}$ for $a_s$ is well within the range of values used by Maraqa (2001) for intermediate-scale and field studies, but lower than the laboratory studies analyzed by Maraqa (2001).

The pesticide study shows that a limited amount of input data could be used to successfully simulate drain discharge rates and chemical concentrations using an equilibrium flow model with composite hydraulic conductivity function, and the mobile-immobile physical nonequilibrium model. The modified soil hydraulic functions in this example provided sufficient flexibility to permit reasonable simulations at the site.

## 15.4 Pore-Scale Modeling

The various modeling applications thus far were based on macroscopic descriptions of the processes involved, notably the Richards equation for variably saturated flow and the advection-dispersion equation for contaminant transport. These equations provide an approximate, large-scale description of the processes involved. In reality, pore-scale physical and geochemical processes govern the fundamental behavior of water and solutes in porous media such as soils and groundwater. The

complexities of these systems, our inability to obtain direct pore-scale observations, and difficulties in upscaling the processes have made it difficult to study porous media at the scale at which the processes occur, and then to extrapolate results to the larger (continuum or Darcy) scale using various upscaling and averaging techniques. For these reasons studies of most multiphase properties (such as the unsaturated soil hydraulic properties and solute dispersion properties) have been based mostly on empirical or quasi-empirical investigations that are inherently limited in detail and applicability.

In an attempt to improve our understanding of multiphase (air-water or air-oil-water) systems, and to develop alternative means of predicting fluid movement, many have turned to pore-scale modeling. As reviewed by Meakin and Tartakovsky (2009), a number of pore-scale modeling approaches are available. Techniques such as traditional grid-based computational fluid dynamics simulation and particle-based Lattice Boltzmann (LB) methods can be used to simulate directly fluid flow and biogeochemical processes within individual pores having realistic complex geometries. In combination with imaging technologies such as X-ray computed tomography (Wildenschild et al. 2002; O'Donnell et al. 2007; Blunt et al. 2013), these modeling techniques can be powerful tools for studying flow and transport processes. However, the models are relatively expensive in terms of computational storage and run-time requirements, particularly for multiphase systems. For these reasons, only limited work has been done modeling real multiphase porous media.

Alternatively, pore network models (PNMs) use idealized representations of complex pore geometries to permit computationally more efficient calculations of water flow and transport processes. PNMs offer a systematic approach for developing improved parametric relationships for the unsaturated soil hydraulic properties, and for simulating fluid flow and contaminant transport processes in homogeneous and heterogeneous media, including multiphase systems. PNMs permit one to focus on pore-scale properties or processes such as residual saturation, interfacial areas, mass transfer rates across interfaces, nonequilibrium transport, the fate of nonaqueous phase liquids (NAPLs), and evaluating alternative methods of simulating single and multiphase flow and transport (Celia et al. 1995; Raoof and Hassanizadeh 2010, 2012). Thus, these models have considerable potential to improve our understanding of the underlying processes, with the end result being improved predictive modeling capabilities and parametric relationships at the larger scale.

Since the seminal work of Fatt (1956), considerable literature has focused on network modeling. It is beyond the scope of the present chapter to present many of the details of pore network modeling techniques. Instead, we consider only briefly a few examples that are indicative of the ways in which pore scale modeling may improve our understanding of multiphase flow and transport processes. More comprehensive reviews are provided by Celia et al. (1995), Meakin and Tartakovsky (2009), and Blunt et al. (2013).

Pore network models (PNMs) can be constructed in various ways, but a typical arrangement consists of relatively large pore bodies located at the nodes of a

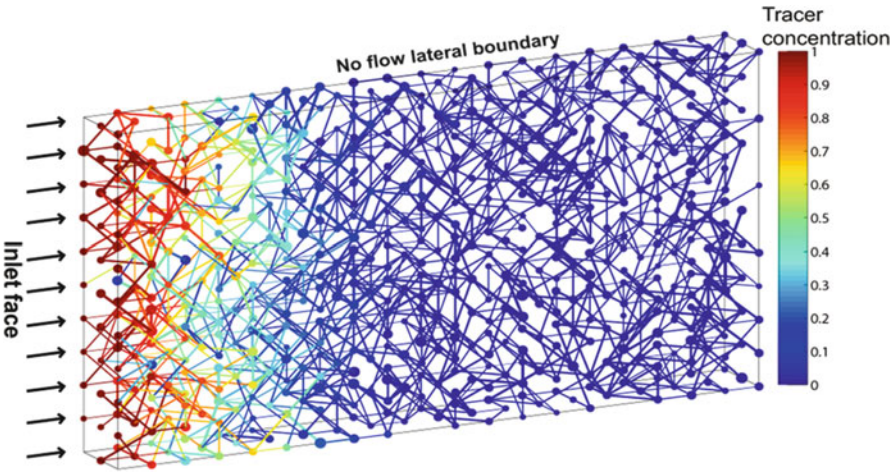


**Fig. 15.12** An example of a pore network domain where a tracer is being injected across the left inlet boundary. The *colors* show the concentration while the *lines* show the pore spaces of the soil

network, with connections between nodes/pores being made by smaller capillary tubes that are referred to as pore throats (Raoof and Hassanizadeh 2010). Due to the use of idealized geometries, it is possible to specify laws or rules for fluid passage in pores and throats, and thereby compute flows in the network for given boundary and initial conditions.

Raoof et al. (2013) recently developed the PoreFlow code for simulating pore scale flow and transport processes. This code may be used to simulate fluid flow and multi-component reactive transport under saturated and variably saturated conditions. The simulated porous medium is created by defining capillary tubes of different sizes (which define the "geometry" of the porous medium) and connecting these in various ways to each other (the "topology" of the porous medium). The fluid flow and solute transport processes of interest are then simulated at the pore scale, with the relevant physics implemented on a pore to pore basis. At this scale, flow and transport are simulated by explicitly modeling the phase interfaces and mass exchange at surfaces. Average values and properties can be obtained by integration over the entire network domain, which provides then also the upscaling relationships. We refer to Raoof and Hassanizadeh (2012) and Raoof et al. (2013) for a detailed discussion of the construction of PNMs, and the mathematical equations used for this purpose.

Figure 15.12 shows an example of a pore network in which solute is being injected across the left side at a given rate. Once PNM calculations are carried out using pore networks of the type shown in this figure, results can be compared with those obtained using a model representing macroscale behavior (such as those based on the Darcy and Darcy-Buckingham laws). This comparison permits one then to study various relationships between the two scales.

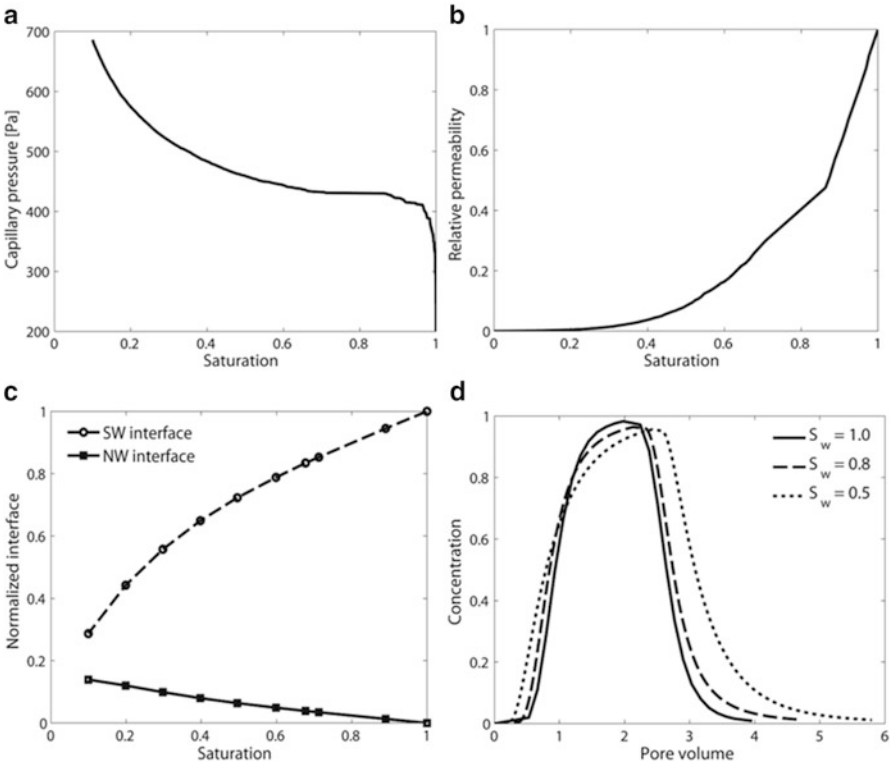


**Fig. 15.13** Pore network modeling results obtained for (**a**) the capillary pressure-saturation curve, (**b**) the relative permeability-saturation curve, (**c**) the normalized total interfacial area of solid-wetting (SW) and nonwetting-wetting (NW) phases as a function of wetting-phase saturation, $S_w$ (the areas are normalized to the total area under saturated conditions, which only belongs to the solid-wetting surfaces), and (**d**) breakthrough curves at three relative saturations

Figure 15.13 shows an application in which the PoreFlow pore network model of Raoof et al. (2013) was used to simulate drainage processes, leading to information about the unsaturated soil hydraulic properties. Results are presented in terms of capillary pressure-saturation and relative permeability-saturation curves, as well as changes in the interfacial areas as a function of relative saturation, $S_w$ ($= \theta/\theta_s$).

Also shown in Fig. 15.13 are PNM calculated solute breakthrough curves obtained for three different values of relative saturation. The curves show higher solute dispersion at lower saturations. These types of results can be used to study the effect of water content and other parameters on solute dispersion. Although dispersion is known to be strongly dependent upon both flow velocity and water content (Maciejewski 1993), not much information exists on the exact nature and functional form of the water content dependency (Bear and Cheng 2008). Many studies have reported higher values of the dispersion coefficient at smaller water contents (Kirda et al. 1973; De Smedt and Wierenga 1984; Maraqa et al. 1997). This effect has been

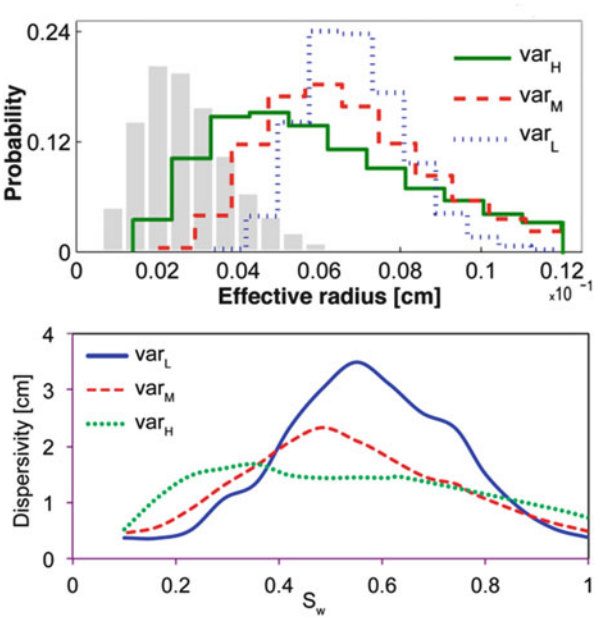


**Fig. 15.14** Distributions of pore-body sizes together with a distribution of pore throat sizes shown as columns (*top*). The pore-body size distributions have different variances: high ($var_H$), medium ($var_M$), and low ($var_L$), representing different soils. The relationship between the dispersivity ($D_L$) and relative saturation ($S_w$) for each pore network is shown in the *bottom* plot

attributed in part to the presence of immobile water (De Smedt and Wierenga 1979, 1984; van Genuchten and Dalton 1986), with the fraction of immobile water likely depending upon the pore structure as well as saturation.

Pore-scale network models are excellent tools for studying these type of immobile water and fluid velocity effects on the dispersion coefficient. Let us restate for this purpose the often-used relationship between the dispersion coefficient and the fluid velocity Eq. 15.15 in a more general form:

$$D(\theta, v) = D_o \tau(\theta) + D_L(\theta)|v|^{\varepsilon} \tag{15.26}$$

where $D_o$ is the diffusion coefficient, $D_L$ is the longitudinal dispersivity, $v$ is the average pore-water velocity ($=q/\theta$) and $\varepsilon$ an empirical constant presumably very close but not necessarily equal to 1.0 under variably saturated conditions (e.g., Kirda et al. 1973; De Smedt et al. 1986). When the water content or relative saturation decreases, travel times and microscopic travel distances tend to become longer, leading to a broader velocity distribution and possibly more dispersion. Consequently, the variability in the microscopic velocity, and its directions at the pore scale, can be (some or much) larger than in saturated porous media, thus increasing tailing in the observed breakthrough curves.

Raoof and Hassanizadeh (2013) used pore network modeling to calculate exactly this saturation dependency of the solute dispersion coefficient for different pore sizes. Results are presented in Fig. 15.14. They indeed show that the dispersivity is

strongly dependent upon relative saturation. The relationship was found to be not monotonic in that a maximum dispersivity occurred at some intermediate saturation value referred to as critical saturation by Raoof and Hassanizadeh (2013). This behavior has been observed also experimentally, most notably by Toride et al. (2003).

Unsaturated dispersion is affected by imperfect solute mixing within pores due to the presence of a nonwetting phase (generally air) and changes in the connectivity among pores. Having a collection of saturated pores may create a relatively fast flow domain overall, while film flow within drained pores together with trapped phases (immobile water) create a relatively slow flow process. Under such a condition, advection-dispersion equation may not accurately simulate transport of solutes at the macro scale and other formulations, such as the mobile-immobile (dual-porosity) model given by Eqs. 15.24a and 15.24b, may become more appropriate for modeling unsaturated solute transport processes.

## 15.5 Concluding Remarks

In this chapter we reviewed a broad range of classical as well as dual-porosity and dual-permeability formulations for modeling equilibrium and nonequilibrium (or preferential) fluid flow and contaminant transport. We focused especially on transport processes in the vadose zone between the soil surface and the groundwater table. A large number of ready-to-use numerical models are now available in both the public and commercials domains. While equilibrium flow and transport models undoubtedly remain applicable to many situations, including macroporous soils and fractured rock when saturated conditions can be avoided, most practical applications may require the use of more parameter-intensive dual-porosity and dual-permeability formulations. As illustrated by the pesticide transport problem, one effective modeling approach requiring far fewer hydraulic parameters is the use of composite (dual-porosity type) functions for the unsaturated hydraulic conductivity to account for the separate effects of macropores and micropores, and then to combine this approach with a mobile-immobile water type nonequilibrium formulation for solute transport. Still, the example shows that preferential flow can have a major effect on the simulation results. The physical nonequilibrium dual-porosity formulation used in this study requires an estimate of the mass transfer coefficient ($\alpha_s$) governing diffusive exchange between the fracture and matrix regions of structured media. While some guidance is provided by literature data, more research is needed to determine the exact scale dependency of this parameter, especially for larger scale field applications. Pore network modeling may well be very useful for studying this scale-dependency, as well as for other lingering problems such as deciphering the effects of fluid velocity and water content on the solute dispersivity.

## References

Assefa KA, Woodbury AD (2013) Transient, spatially varied groundwater recharge modeling. Water Resour Res 49:1–14, doi:10.1002/wrcr.20332

Bear J (1972) Dynamics of fluids in porous media. Elsevier Sci, New York

Bear J, Cheng AHD (2008) Modeling groundwater flow and contaminant transport. Springer, New York

Blunt MJ, Bijeljic B, Dong H, Gharbi O, Iglauer S, Mostaghimi P, Paluszny A, Pentland C (2013) Pore-scale imaging and modelling. Adv Water Resour 51:197–216

Boivin A, Šimůnek J, Schiavon M, van Genuchten MT (2006) Comparison of pesticide transport processes in three tile-drained field soils using HYDRUS-2D. Vadose Zone J 5(3):838–849

Brooks RH, Corey AT (1964) Hydraulic properties of porous media, Hydrol. Paper no 3, Colorado State University, Fort Collins, CO

Celia MA, Reeves PC, Ferrand LA (1995) Recent advances in pore scale models for multiphase flow in porous media. Rev Geophys 33(S2):1049–1057

De Smedt F, Wierenga PJ (1979) Mass transfer in porous media with immobile water. J Hydrol 41 (1):59–67

De Smedt F, Wierenga PJ (1984) Solute transfer through columns of glass beads. Water Resour Res 20(2):225–232

De Smedt F, Wauters F, Sevilla J (1986) Study of tracer movement through unsaturated sand. J Hydrol 85(1):169–181

Durner W (1994) Hydraulic conductivity estimation for soils with heterogeneous pore structure. Water Resour Res 32(9):211–183

Fatt I (1956) The network model of porous media I. Capillary pressure characteristics. Trans AIME 207:144–159

Feddes RA, Kowalik PJ, Zaradny H (1978) Simulation of field water use and crop yield. Wiley, New York

Finsterle S, Doughty C, Kowalsky MB, Moridis GJ, Pan L, Xu T, Zhang Y, Pruess K (2008) Advanced vadose zone simulations using TOUGH. Vadose Zone J 7:601–609

FLMW (1995) Leaching models and EU registration. Guidance document 4952/VI/95, Focus Leaching Modelling Workgroup (FLMW), Commission of the European Communities, Directorate-General for Agriculture VI B II-I, Brussels

Gee GW, Hillel D (1988) Groundwater recharge in arid regions: review and critique of estimation methods. Hydrol Process 2(3):255–266

Gerke HH (2006) Preferential flow descriptions for structured soils. J Plant Nutr Soil Sci 169:382–400

Gerke HH, van Genuchten MT (1993) A dual-porosity model for simulating the preferential movement of water and solutes in structured porous media. Water Resour Res 29:305–319

Gerke HH, van Genuchten MT (1996) Macroscopic representation of structural geometry for simulating water and solute movement in dual-porosity media. Adv Water Resour 19:343–357

Gerke HH, German P, Nieber J (2010) Preferential flow: from the pore to the catchment scale. Vadose Zone J 9(2):207–212

Hanson BR, Šimůnek J, Hopmans JW (2008) Leaching with subsurface drip irrigation under saline, shallow ground water conditions. Vadose Zone J 8:810–818

Hargreaves GH (1975) Moisture availability and crop production. Trans Am Soc Agric Eng 18 (5):980–984

Healy RW (2008) Simulating water, solute, and heat transport in the subsurface with the VS2DI software package. Vadose Zone J. Special Issue "Vadose Zone Modelling" 7:632–639

Hendrickx JMH, Flury M (2001) Uniform and preferential flow, mechanisms in the vadose zone. In: Conceptual models of flow and transport in the fractured vadose zone. National Research Council. National Academy, Washington, DC, pp 149–187

Hopmans JW, Stricker JNM (1989) Stochastic analysis of soil water regime in a watershed. J Hydrol 105:57–84

Jarvis NJ (1994) The MACRO model (Version 3.1), technical description and sample simulations. Reports and Dissertations 19. Department of Soil Science, Swedish University of Agricultural Sciences, Uppsala, Sweden, 51 pp

Jarvis NJ (2007) A review of non-equilibrium water flow and solute transport in soil macropores: principles, controlling factors and consequences for water quality. Eu J Soil Sci 58(3):523–546. doi:10.1111/j.1365-2389.2007.00915.x

Jensen ME, Burman RD, Allen RG (1990) Evapotranspiration and irrigation water requirement, ASCE manuals and reports on engineering practice, vol 70. ASCE, New York

Jimenez-Martinez J, Skaggs TH, van Genuchten MT, Candela L (2009) A root zone modelling approach to estimating groundwater recharge from irrigated areas. J Hydrol 367:138–149

Kandelous MM, Šimůnek J, van Genuchten MT, Malek K (2011) Soil water content distributions between two emitters of a subsurface drip irrigation system. Soil Sci Soc Am J 75(2):488–497

Kirda C, Nielsen DR, Biggar JW (1973) Simultaneous transport of chloride and water during infiltration. Soil Sci Soc Am J 37(3):339–345

Kodesova R, Kozak J, Šimůnek J, Vacek O (2005) Field and numerical study of chlorotoluron transport in the soil profile: comparison of single and dual-permeability model. Plant Soil Environ 51(7):310–315

Köhne JM, Mohanty B, Šimůnek J, Gerke HH (2004) Numerical evaluation of a second-order water transfer term for variably saturated dual-permeability models. Water Resour Res 40. doi:10.1029/2004WR00385

Köhne S, Lennartz B, Köhne JM, Šimůnek J (2006) Bromide transport at a tile-drained field site: experiment, one- and two-dimensional equilibrium and non-equilibrium numerical modeling. J Hydrol 321(1–4):390–408

Köhne JM, Köhne S, Šimůnek J (2009) A review of model applications for structured soils: a) Water flow and tracer transport. J Contam Hydrol. Special Issue "Flow Domains" 104(1–4):4–35. doi:10.1016/j.jconhyd.2008.10.002

Kosugi K (1996) Lognormal distribution model for unsaturated soil hydraulic properties. Water Resour Res 32(9):2697–2703

Larsbo M, Roulier M, Stenemo F, Kasteel R, Jarvis N (2005) An improved dual-permeability model of water flow and solute transport in the vadose zone. Vadose Zone J 4(2):398–406. doi:10.2136/vzj2004.0137

Lazarovitch NJ, Šimůnek J, Shani U (2005) System-dependent boundary condition for water flow from subsurface source. Soil Sci Soc Am j 69:46–50

Leij FJ, Russel WB, Lesch SM (1997) Closed-form expressions for water retention and conductivity data. Ground Water 35(5):848–858

Liu H-H (1998) An active fracture model for unsaturated flow and transport in fractured rocks. Water Resour Res 34:2633–2646

Lu X, Jin M, van Genuchten MT, Wang B (2011) Ground water recharge at five representative sites in the Hebei Plain of China: case study. Ground Water 49(2):286–294

Maciejewski S (1993) Numerical and experimental study of solute transport in unsaturated soils. J Contam Hydrol 14(3):193–206

Mallants D, van Genuchten MT, Simunek J, Jacques D, Seetharam S (2011) Leaching of contaminants to groundwater. In: Swartjes FA (ed) Dealing with contaminated sites; from theory to practical application, Chapter 18. Springer, Dordrecht, pp 787–850

Maraqa MA (2001) Prediction of mass-transfer coefficient for solute transport in porous media. J Contam Hydrol 53:153–171

Maraqa MA, Wallace RB, Voice TC (1997) Effects of degree of water saturation on dispersivity and immobile water in sandy soil columns. J Contam Hydrol 25(3):199–218

Meakin P, Tartakovsky AM (2009) Modeling and simulation of pore-scale multiphase fluid flow and reactive transport in fractured and porous media. Rev Geophys 47(3), RG3002. doi:10.1029/2008RG000263

Millington RJ, Quirk JM (1961) Permeability of porous solids. Trans Faraday Soc 57:1200–1207

Mohanty BP, Bowman RS, Hendrickx JMH, van Genuchten MT (1997) New piecewise-continuous hydraulic functions for modeling preferential flow in an intermittent flood-irrigated field. Water Resour Res 33(9):2049–2063

Narasimhan TN (2005) Buckingham, 1907; an appreciation. Vadose Zone J 4:434–441

Naveira-Cotta CP, Pontedeiro EM, Cotta RM, Su J, van Genuchten MT (2013) Environmental impact assessment of liquid waste ponds in uranium milling installations. Waste Biomass Valoriz 4:197–211. doi:10.1007/s12649-012-9156-0

Neto DC, Chang HK, van Genuchten MTh (2014) Groundwater level and rainfall: A mathematical view of water level variations of the Rio Claro Aquifer, Brazil. Hydrogeol J (submitted)

Novak SM, Banton O, Schiavon M (2003) Modeling metolachlor exports in subsurface drainage water from two structured soils under maize (Eastern France). J Hydrol 270(3–4):295–308

O'Donnell AG, Young IM, Rushton SP, Shirley MD, Crawford JW (2007) Visualization, modelling and prediction in soil microbiology. Nat Rev Microbiol 5(9):689–699

Panday S, Huyakorn PS (2008) MODFLOW SURFACT: a state-of-the-art use of vadose zone flow and transport equations and numerical techniques for environmental evaluations. Vadose Zone J 7:610–631

Peters RR, Klavetter EA (1988) A continuum model for water movement in an unsaturated fractured rock mass. Water Resour Res 24:416–430

Pot V, Šimůnek J, Benoit P, Coquet Y, Yra A, Martínez-Cordón M-J (2005) Impact of rainfall intensity on the transport of two herbicides in undisturbed grassed filter strip soil cores. J Contam Hydrol 8:63–88

Raoof A, Hassanizadeh SM (2010) A new method for generating pore-network models of porous media. Transp Porous Media 81(3):391–407

Raoof A, Hassanizadeh SM (2012) A new formulation for pore-network modeling of two-phase flow. Water Resour Res 48, W01514. doi:10.1029/2010WR010180

Raoof A, Hassanizadeh SM (2013) Saturation-dependent solute dispersivity in porous media: pore-scale processes. Water Resour Res 49:1943–1951. doi:10.1002/wrcr.20152

Raoof A, Nick HM, Hassanizadeh SM, Spiers CJ (2013) PoreFlow: a complex pore-network model for simulation of reactive transport in variably saturated porous media. Comput Geosci 61:160–174

Richards LA (1931) Capillary conduction of fluid through porous mediums. Physics 1:318–333

Rodríguez-Sinobas L, Gil M, Sanchez R, Benitez J (2012) Evaluation of drip and subsurface drip in a uniform loamy soil. Soil Sci 177(2):147–152

Scanlon BR, Healy RW, Cook PG (2002) Choosing appropriate techniques for quantifying groundwater recharge. Hydrogeol J 10(1):18–39

Schaap MG, van Genuchten MT (2006) A modified Mualem-van Genuchten formulation for improved description of the hydraulic conductivity near saturation. Vadose Zone J 5:27–34

Schaap MG, Leij FJ, van Genuchten MT (2001) Rosetta: a computer program for estimating soil hydraulic parameters with hierarchical pedotransfer functions. J Hydrol 251:163–176

Šimůnek J, Bradford S (2008) Vadose zone modeling: introduction and importance. Vadose Zone J. Special Issue "Vadose Zone Modelling" 7(2):581–586

Šimůnek J, van Genuchten MTh (2008) Modeling nonequilibrium flow and transport with HYDRUS. Vadose Zone J. Special Issue "Vadose Zone Modeling" 7:782–797

Šimůnek J, Suarez DL, Šejna M (1996) The UNSATCHEM software package for simulating one-dimensional variably saturated water flow, heat transport, carbon dioxide production and transport, and multicomponent solute transport with major ion equilibrium and kinetic chemistry. Version 2.0. Research Report No. 141, U.S. Salinity Laboratory, USDA, ARS, Riverside, CA, 186 pp

Šimůnek J, Jarvis NJ, van Genuchten MT, Gärdenäs A (2003) Nonequilibrium and preferential flow and transport in the vadose zone: review and case study. J Hydrol 272:14–35

Šimůnek J, van Genuchten MT, Sejna M (2008) Development and applications of the HYDRUS and STANMOD software packages and related codes. Vadose Zone J. Special Issue "Vadose Zone Modelling" 7(2):587–600

Šimůnek J, van Genuchten MTh, Šejna M (2012) The HYDRUS Software package for simulating two- and three-dimensional movement of water, heat, and multiple solutes in variably-saturated media, Technical manual, Version 2.0, PC Progress, Prague, Czech Republic, 258 pp

Šimůnek, Šejna M, Saito H, Sakai M, van Genuchten MTh (2013) The HYDRUS-1D software package for simulating the one-dimensional movement of water, heat, and multiple solutes in variably-saturated media. Version 4.16, HYDRUS Software Series 3, Department of Environmental Sciences, University of California, Riverside, CA, 340 pp

Šimůnek J, Jacques D, Ramos TB, Leterme B (2014) The use of multicomponent solute transport models in environmental analyses. In: Texeira WG, Ceddia MB, Ottono MV, Donnagema GK (eds) Application of soil physics in environmental analyses, Springer (this publication)

Skaggs TH, Trout TJ, Šimůnek J, Shouse PJ (2004) Comparison of HYDRUS-2D simulations of drip irrigation with experimental observations. J Irrig Drain Eng 130:304–310

Skaggs TH, Trout TJ, Rothfuss Y (2010) Drip irrigation water distribution patterns: effects of emitter rate, pulsing, and antecedent water. Soil Sci Soc Am J 74:1886–189. doi:10.2136/sssaj2009.0341

Toride N, Inoue M, Leij FJ (2003) Hydrodynamic dispersion in an unsaturated dune sand. Soil Sci Soc Am J 67(3):703–712

USEPA (2004) Drinking water standards and health advisories. Office of Water, U.S. Environmental Protection Agency (USEPA), Washington, DC, 20 pp

van Dam JC, Groenendijk P, Hendriks RFA, Kroes JG (2008) Advances of modeling water flow in variably saturated soils with SWAP. Vadose Zone J 7:640–635

van Genuchten MT (1980) A closed-form equation for predicting the hydraulic conductivity of unsaturated soils. Soil Sci Soc Am J 44:892–898

van Genuchten MT, Dalton FN (1986) Models for simulating salt movement in aggregated field soils. Geoderma 38:165–183

van Genuchten MT, Wagenet RJ (1989) Two-site/two-region models for pesticide transport and degradation: theoretical development and analytical solutions. Soil Sci Soc Am J 53:1303–1310

van Genuchten MT, Wierenga PJ (1976) Mass transfer studies in sorbing porous media: I. Analytical solutions. Soil Sci Soc Am J 40(4):473–480

van Genuchten MT, Šimůnek J, Leij FJ, Toride N, Šejna M (2012) STANMOD: model use, calibration and validation. Trans ASABE 55(4):1353–1366

Vanderborght J, Kasteel R, Herbst M, Javaux M, Thiéry D, Vanclooster M, Mouvet C, Vereecken H (2005) A set of analytical benchmarks to test numerical models of flow and transport in soils. Vadose Zone J 4(1):206–221. doi:10.2136/vzj2005.0206

Vogel T, van Genuchten MT, Cislerova M (2000) Effect of the shape of the soil hydraulic functions near saturation on variably-saturated flow predictions. Adv Water Resour 24 (2):133–144

Vogel T, Brezina J, Dohnal M, Dusek J (2010) Physical and numerical coupling in dual-continuum modeling of preferential flow. Vadose Zone J 9(2):260–267. doi:10.2136/vzj2009.0091

White MD, Oostrom M, Rockhold ML, Rosing M (2008) Scalable modeling of carbon tetrachloride migration at the Hanford site using the STOMP simulator. Vadose Zone J 7:654–666

Wildenschild D, Vaz CMP, Rivers ML, Rikard D, Christensen BSB (2002) Using X-ray computed tomography in hydrology: systems, resolutions, and limitations. J Hydrol 267(3):285–297

Yeh GT, Salvage KM, Gwo JP, Zachara JM, Szecsody JE (1998) HYDROBIOGEOCHEM: a coupled model of hydrological transport and mixed biochemical kinetic/equilibrium reactions in saturated-unsaturated media. Rep. ORNL/TM-13668, Oak Ridge National Laboratory, Oak Ridge, TN

Zimmerman RW, Chen G, Hadgu T, Bodvarsson GS (1993) A numerical dual-porosity model with semi-analytical treatment of fracture/matrix flow. Water Resour Res 29:2127–2137

Zurmühl T, Durner W (1996) Modeling transient water and solute transport in a biporous soil. Water Resour Res 32:819–829

Zyvoloski GA, Robinson BA, Dash ZV, Trease LL (1997) Summary of the models and methods for the FEHM application – a finite element heat- and mass-transfer code. Los Alamos National Laboratory Rept. LA-13307-MS, Los Alamos, NM